International Journal of Thermophysics, Vol. 19, No. 3, 1998

Adsorption of Hydrogen in Graphitic Slit Pores[1]

Q. Wang[2] and J. K. Johnson[2, 3]

Molecular simulations of adsorption isotherms for hydrogen on graphite and graphitic slit pores are presented. The simulations employ the path integral isomorphism of Feynman to rigorously account for the quantum nature of the adsorbate. The isosteric heat of adsorption of *para*-hydrogen on planar graphite is computed from several different solid–fluid potential models and compared with experiment. The adsorption isotherm for hydrogen on the graphite basal plane was computed at 20 K and compared with experiment. Agreement with experiment is very good. Adsorption isotherms for hydrogen in slit pores of two different pore widths are computed at 20 K and compared with results from classical simulations. Quantum and classical isotherms exhibit qualitatively different behavior.

KEY WORDS: adsorption; graphite; hydrogen; molecular simulation; path integral.

1. INTRODUCTION

Tremendous progress has been made in recent years in accurate molecular modeling of realistic fluids. Algorithmic and computer hardware advances have made possible calculations of free energies, phase equilibria, and adsorption isotherms of moderately complex fluids from a knowledge of the intermolecular potentials. Most of the new algorithms for computing free energies, such as the Gibbs ensemble [1, 2], configurational bias [3–5], and the chain increment [6] methods, have been developed specifically for classical fluids. By classical we mean fluids that both obey Boltzmann statistics and have classical kinetic energy. There are many

[1] Paper presented at the Thirteenth Symposium on Thermophysical Properties, June 22–27, 1997, Boulder, Colorado, U.S.A.

[2] Department of Chemical and Petroleum Engineering, University of Pittsburgh, Pittsburgh, Pennsylvania 15261, U.S.A.

[3] To whom correspondence should be addressed.

0195-928X/98/0500-0835$15.00/0

systems of scientific and technological interest that cannot be treated classically. Hydrogen and helium are two fluids that exhibit important deviations from classical behavior. In this paper we restrict our scope to conditions where classical (Boltzmann) statistics may be invoked, but where the kinetic energy must be treated quantum mechanically.

The path integral formalism due to Feynman [7] provides a theoretical framework for describing quantum systems in terms of a classical isomorphism. In essence, the path integral formalism says that the equilibrium statistical mechanics of a quantum system can be mapped onto a classical many-body system of ring polymers, with each ring polymer containing P beads. Strictly speaking, this isomorphism is exact only in the limit of an infinite number of beads per ring, but for most finite temperature systems, essentially exact results can be obtained with bead numbers ranging from tens to hundreds. For the conditions considered in this work, we are able to use about 40 beads or fewer. Sampling the properties of the system of ring polymers can be accomplished through Monte Carlo or molecular dynamics techniques, and the resulting properties can be mapped back onto the quantum system. We have used multiple time-step hybrid Monte Carlo [8] to evaluate the statistical mechanics of the ring polymer fluid.

We present calculations for the isosteric heat of adsorption and adsorption isotherms for hydrogen on planar graphite and compare our results with experiment. Adsorption isotherms for hydrogen in graphite slit pores are computed and compared with results from classical simulations.

2. THEORY AND MODEL

In previous papers we have derived extensions of the path integral hybrid Monte Carlo (PIHMC) method to the Gibbs and grand canonical ensembles [9–11]. The grand canonical Monte Carlo (GCMC) path integral method is used here for computing adsorption isotherms of hydrogen on graphite.

In the path integral formalism, each quantum molecule is replaced by a classical ring polymer of P beads. Each bead is bonded to the neighboring beads in the ring by harmonic springs. The polymers experience both an external potential U^{ext}, due to the other molecules in the system, including the solid–fluid adsorption potential, and an internal potential U^{int}, which comes from the intramolecular bonding interactions. The external potential is given by

$$U^{\text{ext}} = \frac{1}{P} \sum_{\alpha=1}^{P} \sum_{i<j}^{N} V(r_{ij}^{\alpha}) + \frac{1}{P} \sum_{\alpha=1}^{P} \sum_{i}^{N} V_{\text{sf}}(z_i^{\alpha}), \tag{1}$$

where P is the number of beads in each ring, N is the total number of molecules, $V(r_{ij}^{\alpha})$ is the pair potential between bead α on molecule i and bead α on molecule j, r_{ij}^{α} is the scalar distance between the beads, $V_{sf}(z_i^{\alpha})$ is the interaction energy between bead α on molecule i and the solid surface, and z_i^{α} is the distance between bead α and the solid surface. The internal potential is in the form of a harmonic potential,

$$U^{\text{int}} = \frac{Pm}{2(\beta h)^2} \sum_{\alpha=1}^{P} \sum_{i=1}^{N} |\vec{r}_i^{\alpha} - \vec{r}_i^{\alpha+1}|^2 \tag{2}$$

where $\vec{r}_i^{\alpha}$ is the position of bead α on ring i, m is the mass of the quantum molecule, $\beta = 1/kT$, k is the Boltzmann constant, T is the absolute temperature, and $h = h/2\pi$, where h is the Planck constant.

The GCMC algorithm involves three types of moves [12], namely, particle displacements, particle creations, and particle deletions. In a particle creation step, conformations of the inserted molecule are sampled from the ideal gas ring polymer fluid. The creation move is accepted with a probability of

$$\mathscr{P}^{\text{create}} = \min\left(1, \frac{V \exp[\beta(\mu - u_{\Gamma}^{\text{ext}})]}{(N+1)\,\Lambda^3}\right) \tag{3}$$

where μ is the chemical potential, V is the volume of the simulation box, $\Lambda = (2\pi mkT/h^2)^{-1/2}$ is the thermal wavelength, Γ represents the conformation of the molecule inserted into the box, and u_{Γ}^{ext} is the interaction of the inserted molecule with all the molecules in the fluid and solid surface. Note that only the external energy appears since the change of the internal energy is canceled with the internal energy in the probability of choosing the conformation [11]. Similarly, the probability of accepting an attempted deletion is

$$\mathscr{P}^{\text{delete}} = \min\left(1, \frac{N\Lambda^3}{V} \exp[\beta(u_{\Gamma}^{\text{ext}} - \mu)]\right) \tag{4}$$

where Γ represents the conformation of the molecule deleted from the box, and u_{Γ}^{ext} is the interaction of the deleted molecule with the remaining $N-1$ molecules and the solid surface.

We have used the Silvera–Goldman potential [13] to describe the hydrogen–hydrogen interactions. This potential has been shown to reproduce accurately the thermodynamic properties of fluid hydrogen over a wide temperature and pressure range [9, 10].

The solid–fluid potential is of primary importance for modeling adsorption phenomena. We have used four potentials in our simulations,

namely, two different parameterizations of the 10–4–3 potential [14], the Mattera potential [15], and the Crowell–Brown potential [16]. The 10–4–3 potential assumes that the solid–fluid interaction can be modeled by the Lennard–Jones potential. The parameters for the 10–4–3 potential were obtained by using the standard parameters for carbon [14] in combination with two different sets of fluid–fluid hydrogen parameters and the Lorentz–Berthelot combining rules. The fluid hydrogen parameters used are due to Buch [17], $\sigma_{ff} = 2.96$ Å, $\varepsilon_{ff}/k = 34.2$ K, and Silvera–Goldman [13], $\sigma_{ff} = 3.003$ Å, $\varepsilon_{ff}/k = 32.21$ K. The Silvera–Goldman parameters are "effective" Lennard–Jones parameters, obtained by setting ε_{ff} to the well depth of the Silvera–Goldman potential and setting σ_{ff} equal to the distance at which the potential is zero. The Mattera [15] and Crowell–Brown [16] potentials, like the 10–4–13 potential, are also averaged solid–fluid potentials.

We have calculated the isosteric heats of adsorption in order to evaluate the different solid–fluid potentials. The isosteric heat of adsorption can be obtained in a GCMC simulation from the fluctuations of the number of particles and the total energy [18].

$$Q_{st} = RT - \frac{\langle EN \rangle - \langle E \rangle \langle N \rangle}{\langle N^2 \rangle - \langle N \rangle^2} \tag{5}$$

where Q_{st} is the isosteric heat of adsorption per molecule, R is the universal gas constant, and E is the total energy, which is the sum of potential and kinetic energies.

3. SIMULATION DETAILS

We have used the multiple time-step PIHMC algorithm [8] to accomplish the molecular displacements. All molecules in the simulation cell are moved in a single PIHMC displacement. A single MC displacement move typically consists of 5 to 10 long time-steps. The value of the long time-step was adjusted during equilibration to give an acceptance rate of roughly 50%. Each long time-step consists of ten short time-steps in our simulations. Details of the multiple time-step PIHMC simulations are given in our previous papers [9–11]. In the molecule creation step a path is inserted in the box with a random position and random orientation. The conformation of the inserted molecule is randomly picked from the conformations of the ideal gas ring polymer system. Conformations of the ideal gas system were generated as in previous bulk GCMC and Gibbs ensemble simulations [10, 11]. The probabilities of making a displacement, a molecule creation, or a deletion were set to 0.1, 0.45, and 0.45, respectively.

The path integral GCMC simulations were carried out in a simulation box with fixed values of box volume, chemical potential, and temperature. Periodic boundary conditions in x and y directions were used. The bead–bead intermolecular cutoff was maintained at 5 σ_{ff}. The lateral dimension of the box $L_x(L_y)$ was set to be larger than 10 σ_{ff}. No fluid–fluid long range corrections were applied to the configurational properties. We have also performed classical GCMC simulations, but because hybrid Monte Carlo is not efficient for classical systems, the displacement step was accomplished by the standard Metropolis algorithm [19].

For modeling adsorption on a graphite basal plane, one wall of the box was chosen as the adsorbing surface, and the other wall was chosen to be repulsive in order to keep the molecules in the box. The two walls were separated by a large enough distance so that the influence of the repulsive wall on adsorption properties was negligible. The distance between the two walls was always larger than 6 σ_{ff} in our simulations. The reduced volume of the simulation box (V/σ_{ff}^3) was set to 600 to 30,000, which gave average numbers of molecules ranging from 50 to 150. Simulations were usually started from the final configurations of earlier simulations at lower chemical potentials. When no earlier configurations were available, the simulations were started with the centers of mass of the hydrogen molecules on a fcc lattice and the beads of each molecule coincident with the molecule center. The z coordinate of each molecule was scaled so that the molecules were away from the adsorbing wall and hard wall. For simulations starting from the fcc lattice, the molecules were equilibrated for 1000 molecular dynamics steps to melt the lattice and expand the particles into rings before any creation or deletion moves were attempted. The system was equilibrated for about 5 to 10×10^4 PIHMC steps, after which data were collected for 5 to 10×10^4 steps. As the system approached full monolayer coverage, many more PIHMC moves were needed to reach equilibrium. This is because creation and deletion moves become much less efficient near monolayer coverage. Near monolayer coverage we used 2×10^5 trials to achieve equilibrium, and 2×10^5 for data collecting. The amount of hydrogen in the middle of the simulation box was found to be negligible compared with the amount of hydrogen adsorbed on the graphite basal plane at 20 K. This allowed us to approximate the excess adsorption with the total number of hydrogen molecules adsorbed on the graphite surface. We used 32 beads per ring polymer at 20 K.

We have calculated the adsorption of hydrogen in carbon slit pores with pore widths of 3.5 and 5 σ_{ff} at 20 K using 32 beads per molecule. The slit-like pore was modeled by two parallel graphite basal planes separated by the pore width H. The pore width is defined as the distance between the nuclei of carbon atoms in the first layer of each of the planes. The lateral

length of the pore walls was chosen to be from 10 to 20 σ_{ff}, which gave an average number of molecules of about 100 to 300. The initial configurations are chosen in the same way as adsorption on basal plane. Typically, 8 to 12×10^4 PIHMC steps were used for equilibration and 6 to 8×10^4 steps were used for data collection. More than 1.5×10^5 steps are needed to reach equilibrium when the system approaches full monolayer coverage and capillary condensation.

4. RESULTS AND DISCUSSION

We have calculated the isosteric heat of adsorption for *para*-hydrogen at 20 K using four hydrogen–graphite potentials. The adsorption isotherm of hydrogen on the graphite basal plane has been computed at 20 K. The calculations from simulations are compared with data from experiment. We have calculated the hydrogen adsorption in carbon slit pores with two different pore widths at 20 K. The quantum effects on the hydrogen adsorption are assessed by comparing classical calculations with quantum calculations.

4.1. Isosteric Heats of Adsorption

We have plotted the isosteric heats of adsorption for *para*-hydrogen on the graphite basal plane from our simulations using the Crowell–Brown potential [16] in Fig. 1, along with experimental data [20]. Both experiment and simulation show a sharp decrease in the heat of adsorption as the first layer becomes filled. However, the experimental heat of adsorption is fairly constant before first layer filling, while the simulation data show an increase in the heat of adsorption before the drop due to filling of the first layer. The increase can be explained in terms of the increased attractive interactions with the fluid molecules already adsorbed on the surface as the coverage increases, but before the first layer is filled. The error bars on the simulation data become very large as the first layer becomes filled because the probability of successfully creating or deleting a molecule becomes small. Results from simulations with other solid-fluid potentials were qualitatively similar to the data shown in Fig. 1. The experimental isosteric heat at zero coverage [20] was estimated to be the value at a fractional coverage of 0.2. This gives a value of 910 cal $\cdot$ mol^{-1} for *para*-hydrogen. However, other estimates of the isosteric heat at zero coverage range from 1293 [21] to 1180 cal $\cdot$ mol^{-1}. Extrapolation of the simulation data to zero coverage gives values of 1037, 946, 853, and 842 cal $\cdot$ mol^{-1} for the Mattera, Crowell–Brown, 10–4–3 with the Buch and Silvera–Goldman parameters,

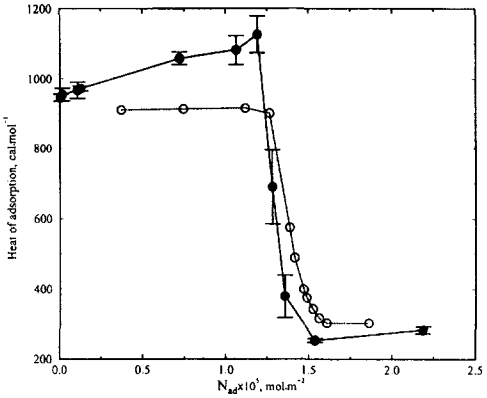

Fig. 1. Isosteric heats of adsorption for *para*-H_2 on graphite from the Crowell–Brown potential at 20.4 K. The filled circles are from path integral simulations, and the open circles are experimental data [20].

respectively. The results from the Crowell–Brown potential give the best agreement with the experimental data of Pace and Siebert [20].

4.2. Adsorption on the Graphite Basal Plane

We have computed adsorption isotherms from path integral GCMC simulations for parahydrogen adsorbed on the graphite basal plane, using the Mattera potential [15]. We have chosen to use the Mattera potential because it gave the best agreement with experimental adsorption data at 20 K, although its isosteric heat at zero coverage was the highest of the potentials examined. Adsorption isotherms for 20 K from experiments and simulations are presented in Fig. 2. The simulation data are shown as filled circles, while experimental data are denoted by open circles. The simulation data are in good agreement with experiment, although the simulations give systematically lower amounts adsorbed. The isotherm shows a gradual, incomplete formation of the second layer.

4.3. Hydrogen Adsorption in Carbon Slit Pores

In Figs. 3 and 4, results of path integral and classical GCMC simulations for the adsorption of hydrogen in slit graphite pores of width $H^* = H/\sigma_{ff} = 3.5$ and $H^* = 5$ at 20 K are presented. The quantum simulations are denoted by the filled circles, and the classical results correspond

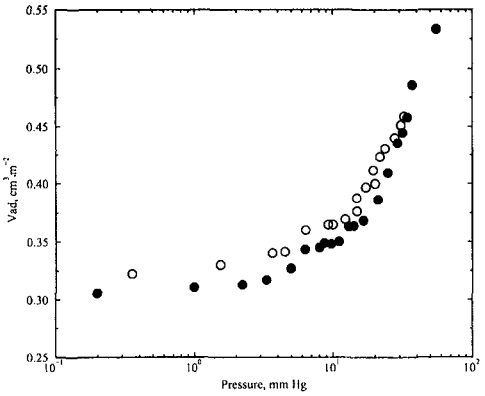

Fig. 2. Adsorption isotherms for *para*-H_2 on basal plane graphite at 20 K. The filled circles are data from path integral simulations, and the open circles are experimental data [23].

to the open circles. From Figs. 3 and 4, we see a continuous filling of the first two adsorbed layers for the quantum simulations. In contrast, the classical simulations give an indication of a first-order transition for the filling of the first layer on each plane. The classical simulations for both $H^* = 3.5$ (Fig. 3) and $H^* = 5$ (Fig. 4) show that capillary condensation

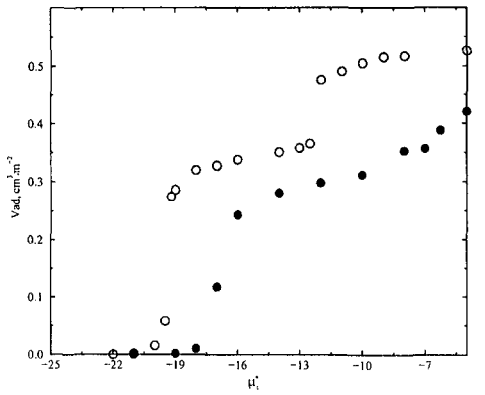

Fig. 3. Adsorption isotherms for *para*-H_2 in a carbon slit pore of width $H^* = 3.5$ at 20 K. The filled circles are from path integral simulations, and the open circles are from classical simulations. $\mu_c^* = \mu_c/\varepsilon$, where μ_c is the configurational chemical potential.

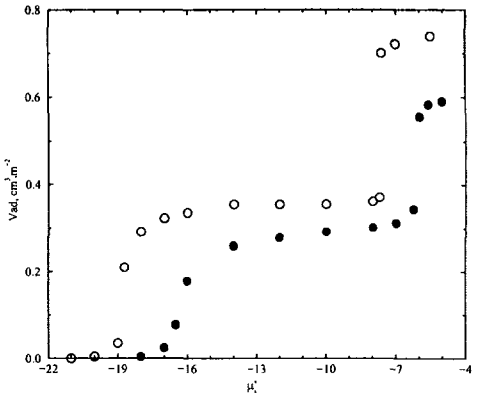

Fig. 4. Adsorption isotherms for *para*-H_2 in a carbon slit pore of width $H^* = 5$ at 20 K. The filled circles are from path integral simulations, and the open circles are from classical simulations. $\mu_c^* = \mu_c/\varepsilon$, where μ_c is the configurational chemical potential.

occurs at 20 K. For the $H^* = 3.5$ pore, this corresponds to filling a third layer in the center of the pore. For $H^* = 5$, two inner layers are formed in the center of the pore, for a total of four layers in the filled pore. However, the quantum simulations show that the third layer for $H^* = 3.5$ fills continuously, and does not exhibit capillary condensation. The quantum simulations for the $H^* = 5$ slit pore do show capillary condensation as the middle two layers fill. This behavior can be explained in terms of the effective radius of the quantum molecule being larger than that of the classical particle. Thus, the $H^* = 3.5$ pore is not quite wide enough to accommodate three layers, and capillary condensation is suppressed. The $H^* = 5$ pore is wide enough to accommodate four layers of the quantum fluid, hence, capillary condensation is observed.

5. CONCLUSIONS

We have presented calculations for the isosteric heats of adsorption and adsorption isotherms for hydrogen on graphite. We have accounted for the quantum motion of the hydrogen nuclei through the path integral formalism of Feynman. We have compared isosteric heats of adsorption and adsorption isotherms from simulations with experiment and have found good agreement. We have computed adsorption isotherms for hydrogen in graphitic slit pores of two different widths; Comparison of quantum and classical simulations shows that capillary condensation can be suppressed

in quantum fluids because of the larger effective diameter of the quantum molecules.

ACKNOWLEDGMENTS

We thank the donors of The Petroleum Research Fund, administered by the American Chemical Society, and the Office of Naval Research for partial support of this work.

REFERENCES

1. A. Z. Panagiotopoulos, *Mol. Phys.* **61**:813 (1987).
2. A. Z. Panagiotopoulos, N. Quirke, M. Stapleton, and D. J. Tildesley, *Mol. Phys.* **63**:527 (1988).
3. J. I. Siepmann and D. Frenkel, *Mol. Phys.* **75**:59 (1992).
4. J. J. dePablo, M. Laso, and U. W. Suter, *J. Chem. Phys.* **96**:2395 (1992).
5. J. J. dePablo, M. Laso, and U. W. Suter, *J. Chem. Phys.* **96**:6157 (1992).
6. S. K. Kumar, I. Szleifer, and A. Z. Panagiotopoulos, *Phys Rev. Lett.* **66**:2935 (1991). S. K. Kumar, *J. Chem. Phys.* **96**:1490 (1992).
7. R. P. Feynman and A. R. Hibbs, *Quantum Mechanics and Path Integrals* (McGraw-Hill, New York, 1965).
8. M. E. Tuckerman, B. J. Berne, G. J. Martyna, and M. L. Klein, *J. Chem. Phys.* **99**:2796 (1993).
9. Q. Wang, J. K. Johnson, and J. Q. Broughton, *Mol. Phys.* **89**:1105 (1996).
10. Q. Wang and J. K. Johnson, *Fluid Phase Equil.* **132**:93 (1997).
11. Q. Wang, J. K. Johnson, and J. Q. Broughton, *J. Chem. Phys.* **107**:5108 (1997).
12. G. E. Norman and V. S. Filinov, *High Temp. USSR* **7**:216 (1969).
13. I. F. Silvera and V. V. Goldman, *J. Chem. Phys.* **69**:4209 (1978).
14. W. A. Steele, *Surf. Sci.* **36**:317 (1973).
15. L. Mattera, C. S. Rosatelli, F. Tommasini, U. Valbusa, and G. Vidali, *Surf. Sci.* **93**:515 (1980).
16. A. D. Crowell and J. S. Brown, *Surf. Sci.* **123**:296 (1982).
17. V. Buch, *J. Chem. Phys.* **100**:7610 (1984).
18. D. Nicholson and N. G. Parsonage, *Computer Simulation and the Statistical Mechanical Theory of Adsorption* (Academic Press, London, 1982).
19. M. P. Allen and D. J. Tildesley, *Computer Simulation of Liquids* (Clarendon, Oxford, 1987).
20. E. L. Pace and A. R. Siebert, *J. Phy. Chem.* **63**:1398 (1959).
21. G. Constabaris, Jr., J. R. Sams, and G. D. Halsey, Jr., *J. Phys. Chem.* **65**:367 (1961).
22. J. Dericbourg, *Surf. Sci.* **59**:565 (1976).
23. J. G. Daunt, S. G. Hegde, and S. P. Tsui, *J. Low Temp. Phys.* **44**:207 (1981).